


Amorphous Phase Formation and Heat Treating Evolution in Mechanically Alloyed Ti–Cu Alloy for Biomedical Applications

P. Urban¹  · R. Astacio¹ · F. Ternero¹ · L. Náhlík² · J. Cintas¹

Received: 5 April 2022 / Accepted: 8 July 2022 / Published online: 27 July 2022
© The Author(s) 2022

Abstract The present work aims to produce Ti_xCu_{100-x} ($x=90, 80, 70,$ and 60) amorphous alloys by using high energy ball mill. The microstructure and possible formation of amorphous phases were characterized employing laser granulometry, scanning electron microscopy (SEM), transmission electron microscopy (TEM), and X-ray diffraction (XRD). The amorphous-crystalline transformation at high temperatures was studied according to differential scanning calorimetry (DSC) and XRD. The $Ti_{80}Cu_{20}$ alloys were obtained in an amorphous state after 30 h of mechanical alloying, and the amorphous phase is stable up to 340 °C. At higher temperatures, this alloy crystallizes, forming the intermetallic compound Ti_2Cu , and a substitutional solid solution $Ti(Cu)$.

Keywords Amorphization · Crystallization · Mechanical alloying · Titanium · Copper

1 Introduction

Amorphous metals and alloys (also known as metallic glasses) have represented a new advance in metallic materials. In 1960, at the California Institute of Technology (Caltech) in the USA, the first metallic glass, $Au_{75}Si_{25}$ [1] alloy, produced by rapid solidification process (RSP), was manufactured. Subsequently, other techniques such as

mechanical alloying (MA) [2–5], plasma spraying [6], sputtering [7], or melt spinning [8] have been shown to produce this type of materials.

Unlike traditional crystalline alloys, amorphous metals have a homogeneous composition and a short-to-medium range order. That is why they have excellent mechanical [9–11], optical [12], and chemical [13, 14] properties. Due to their unique properties, amorphous metals have been investigated as promising candidates in multiple applications such as sporting goods [15], jewellery and watchmaking industries [16], optical components [17], magnetic cores for transformers [18], high-speed motor parts [19], pressure sensors [20], surface coating materials [21], knives for ophthalmology [22], nerve tissue regeneration application [23] and many others. Especially in the last 20 years, amorphous alloys have attracted wide attention from the scientific community and international industry, being one of the most active research areas in the materials field.

In the last ten years, Ti-Cu-based crystalline alloys have been intensively studied for their high specific strength [24], good mechanical properties [25, 26], good tribological properties [27], good plasticity [29], good biocompatibility [25] and good bio-corrosion [26] and antibacterial properties [26–28] for biomedical applications.

An additional possibility to improve the properties of the Ti-Cu crystalline alloys is to produce amorphous/nanocrystalline Ti-Cu alloys. Until now, several authors have manufactured different Ti-Cu amorphous alloys in powder or ribbon form by different methods (Table 1). Only one study is similar to ours. Politis and Johnson [35] synthesized amorphous alloys over a titanium content range of 13–90 at.% by mechanical alloying. However, the conditions of the mechanical alloying are different and the results have not been verified by TEM. Only XRD and DSC technique have been used to verify the presence of the amorphous phase and

✉ P. Urban
purban@us.es

¹ Department of Materials Science and Transportation, Escuela Técnica Superior de Ingeniería, Universidad de Sevilla, Camino de los Descubrimientos s/n, 41092 Seville, Spain

² Institute of Physics of Materials, Czech Academy of Sciences, Žitkova 22, 616 62 Brno, Czech Republic

Table 1 Different methods of preparation and compositions of amorphous Ti_xCu_{100-x} alloys

Ref	Preparation	Amorphous range
*	Mechanical alloying	$x = 80$
[30]	Melt spinning	$0.25 \leq x \leq 0.72$
[31]	Mechanical alloying	$x = 20, 35, 40$
[32]	Mechanical alloying	$x = 36$
[33]	Mechanical alloying	$x = 45, 50, 55$
[34]	Mechanical alloying	$x = 50$
[35]	Mechanical alloying	$x = 13-90$

*Present investigation

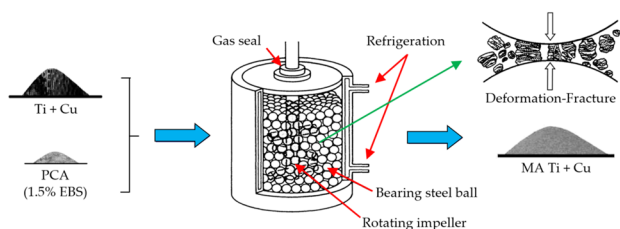
these techniques cannot distinguish between an amorphous and a nanocrystalline phase. In addition, there is no mention about the evolution of amorphous powder during heating and what phases are formed.

The most important problem of amorphous powders is how they can be sintered without losing the amorphous phase. We have carried out additional studies of consolidation by electrical resistance sintering [10]. Results will be reported in a future publication.

2 Material and Methods

Pure titanium powder Se-Jong 4 and pure copper powder CH-L10 were mixed to achieve $Ti_{90}Cu_{10}$, $Ti_{80}Cu_{20}$, $Ti_{70}Cu_{30}$, and $Ti_{60}Cu_{40}$. The mixed powder was put into a high-energy attritor ball mill (Fig. 1) and then mechanically alloyed through high speed collisions using stainless steel vial (3 l) and balls (0.5 mm diameter). To avoid the oxidation of the powder during ball milling, the process was carried out in an Ar atmosphere. The ball to powder mass ratio was 20:1 (72 g of powder), and the rotational speed was 500 rpm. Milling was interrupted after 1, 5, 10, 15, 20, 30, 40, 50, and 60 h to take a sample of milled powder.

The as-mixed powders and powders milled for different times have been characterized by laser granulometry, scanning electron microscopy (SEM), transmission electron

**Fig. 1** Scheme of the amorphization procedure by mechanical alloying

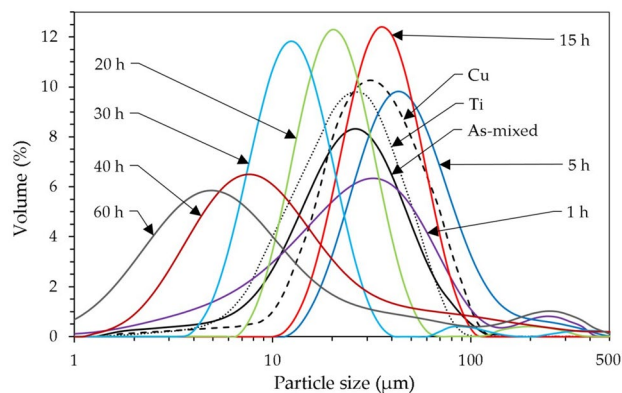
microscopy (TEM), and differential scanning calorimetry (DSC).

3 Results and Discussion

3.1 Characterization of Particles Morphology

The granulometric results obtained for the $Ti_{80}Cu_{20}$ alloy are shown in Fig. 2. Each of the curves corresponds to the granulometric analysis of the as-received Cu and Ti powder particles and the samples taken for different hours of milling. Under normal conditions, during the mechanical alloying, two different effects can occur: welding or fragmentation of the particles. The particles that are usually welded are the ductile ones, and those that are fragmented are the brittle ones.

The as-mixed curve corresponds to the mixture of titanium and copper powder in the received state. The value of the volume median diameter, $D(0.5)$, is $28.19 \mu m$. The 10% of the volume distribution, $D(0.1)$, is below $12.21 \mu m$, and 10% of the volume distribution, $D(0.9)$, is above $58.43 \mu m$. The curve corresponding to 1 h milling is slightly displaced to right as compared with that of the as-mixed powders. It is due to the predominance of welding over particle fragmentation during the first stages of milling. The welding of the powders continues to be the predominant factor up to 5 h of milling, as it appears in Fig. 2. After this period, the curves start shifting to the left, which indicates that the fracturing of the particles predominates over the welding. The particles, mainly copper, have been strain-hardened to such a degree that fracturing is more likely than welding. Between 15 and 30 h of milling, the curves become sharper. The welding domain is declining, and the larger particles are fragmented. The size of the particles becomes smaller, and the range of sizes is more homogeneous.

**Fig. 2** Granulometric curves of as-mixed and mechanically alloyed $Ti_{80}Cu_{20}$ powders for different milling times

For the curves at 20 and 30 h, respectively, there is already a clear domain of fragmentation since they are shifting markedly to the left, maintaining a relatively small range of sizes. After 40 h of milling, the curve's width increases considerably, and the size of the particles continue to decrease. In addition, some smaller particles with higher surface energy suffer agglomeration, forming larger particles. Finally, the smallest particles are formed after 60 h of milling with the volume median diameter $D(0.5)$ equal to $5.81 \mu\text{m}$.

Regarding the rest of the alloys, before milling, the $D(0.5)$ of the different mixtures are very similar (Fig. 3) since pure copper and titanium have very similar particle sizes with values of $30.28 \mu\text{m}$ and $22.24 \mu\text{m}$, respectively. In all cases, in the first hours of milling, when the welding process is predominant, more significant differences in particle size are observed between different alloys. These differences reach a maximum around 5 h of milling. In the alloys with more copper content, the particle size increases faster, and with 5 h of milling, the values of $D(0.5)$ for $\text{Ti}_{90}\text{Cu}_{10}$ and $\text{Ti}_{60}\text{Cu}_{40}$ are $43.51 \mu\text{m}$ and $75.13 \mu\text{m}$, respectively. After 5 h, due to the intense fragmentation of the particles, the particle size decreases considerably until the end of the milling. After 60 h, the particles in all alloys have a very homogeneous size $D(0.5)$ that ranges from $5.32 \mu\text{m}$ to $8.36 \mu\text{m}$.

Scanning electron microscopy (SEM), using SE, BSE and EDX detectors, was employed to observe powders particles' morphology and composition. Pure titanium and copper powders can be seen in Fig. 4a. Their different atomic weight (63.55 and 47.87 g/mol for Cu and Ti, respectively) enable their differentiation using the BSE detector. Titanium particles appear darker due to their lower atomic weight. It can be seen that the copper particles have their characteristic dendritic shape due to the manufacturing process to obtain this powder. Titanium particles, on the other hand, are irregular and angular in shape.

After milling the $\text{Ti}_{80}\text{Cu}_{20}$ mixture for 1 h (Fig. 4b), the particles have a much flatter structure. It is due to the effect of plastic deformation caused by the impacts of the

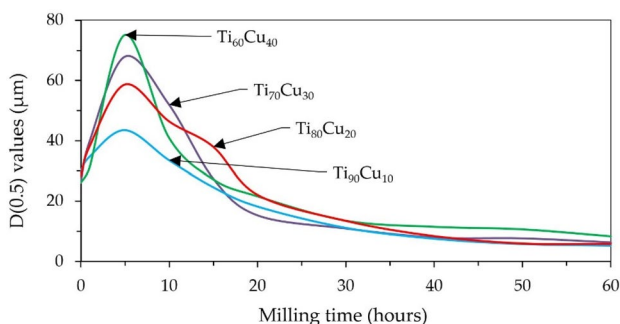


Fig. 3 $D(0.5)$ values of the different Ti-Cu alloys milled for different times

milling balls. In addition to this, copper and titanium have entirely lost their dendritic and angular shape, respectively. After milling the mixture for 5 h (Fig. 4c), the particles are rounded and have a more homogeneous shape, being practically impossible to distinguish titanium from copper. Due to the effect of welding, the particles' $D(0.5)$ size increases to a value of $58.64 \mu\text{m}$. 80% of the particles have sizes between 24.61 and $108.34 \mu\text{m}$. After 5 h of milling, the effect of the fragmentation of the particles begins to predominate due to their higher hardness. Finally, after 60 h of milling (Fig. 4d), the particles have a spherical shape with a size of approximately $5 \mu\text{m}$. The high surface energy of these tiny particles causes them to form agglomerates with sizes up to tens and hundreds of microns.

EDX detector was employed to determine powder particles' composition of $\text{Ti}_{80}\text{Cu}_{20}$ alloy milled for 30 h (Fig. 4e). At both EDS spots and in the selected area, the composition is very similar to the composition of the alloy. The composition of the particles is very homogeneous and practically all the particles have an almost spherical shape. The Pt peaks belong to the platinum coating during the preparation of the samples for SEM.

In alloys with a higher quantity of copper, up to 5 h of milling, the particle size increases with greater intensity in the welding stage. After milling the $\text{Ti}_{60}\text{Cu}_{40}$ alloy for 5 h (Fig. 4f), the particles reach $D(0.5)$ of $75.13 \mu\text{m}$. 80% of the particles have sizes between 46.62 and $215.33 \mu\text{m}$.

All alloys milled for 60 h have particles with a very similar spheroidal shape (Fig. 4d and g) and with $D(0.5)$ sizes between 5.32 and $8.36 \mu\text{m}$, as previously mentioned.

3.2 Microstructure of Milled Powders

The XRD analysis has been used to determine if the milled powders present any crystalline, nanocrystalline, or amorphous phase. In all the diffractograms of the $\text{Ti}_{90}\text{Cu}_{10}$ (Fig. 5a), $\text{Ti}_{80}\text{Cu}_{20}$ (Fig. 5b), $\text{Ti}_{70}\text{Cu}_{30}$ (Fig. 5c), and $\text{Ti}_{60}\text{Cu}_{40}$ alloys (Fig. 5d), it is observed that during the first 15 h of milling, as the milling time increases, the intensity of the peaks corresponding to Ti (JCPDS Number: 00–044–1291) and Cu (JCPDS Number: 00–004–0836) decreases. At the same time, the width of the peaks increases considerably due to the decrease in crystallite size. After 15 h of milling, in the alloys with 90, 70, and 60 at% Ti, only a broad peak with little intensity at 40° remains present, indicating the presence of some crystalline phase. Furthermore, in alloys with 90 and 70 at% Ti, a small peak, located at about 63° , can be observed, which belongs to pure titanium or the solid solution $\text{Ti}(\text{Cu})$.

In the $\text{Ti}_{80}\text{Cu}_{20}$ alloy (Fig. 5b), after 5 h of milling, the amorphous phase begins by atomic diffusion between the Ti and Cu. Thus, after 15 h, independent peaks of Ti and Cu cannot be observed, but a broad peak characteristic of

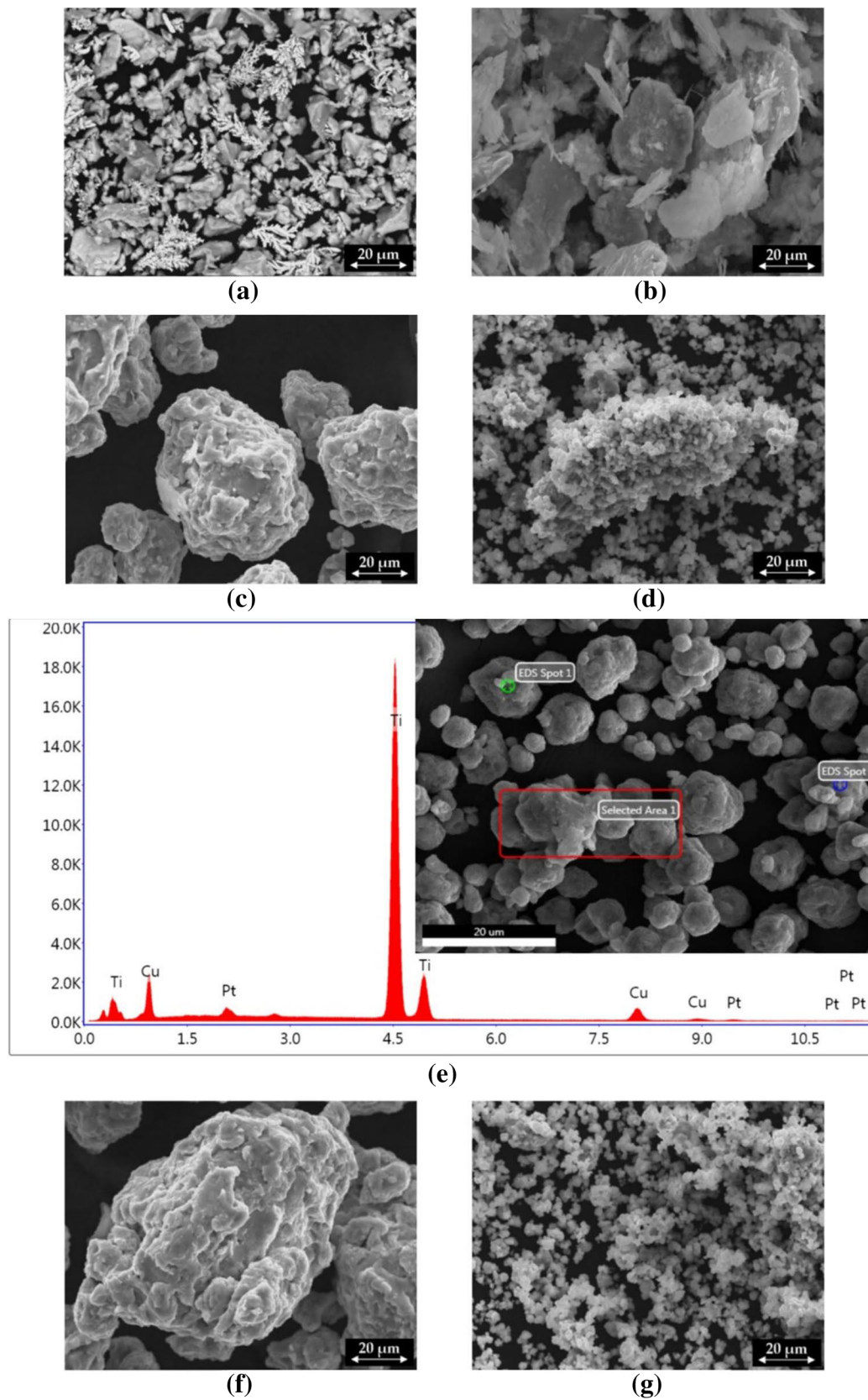


Fig. 4 SEM images of $\text{Ti}_{80}\text{Cu}_{20}$ (a) as-mixed powders (BSE detector), and milled for (b) 1, c 5, and d 60 h (SE detector). e SEM–EDX analysis of $\text{Ti}_{80}\text{Cu}_{20}$ powders milled for 30 h in the spot 1, SEM images (SE detector) of $\text{Ti}_{60}\text{Cu}_{40}$ powders milled for (f) 5 h and g 60 h

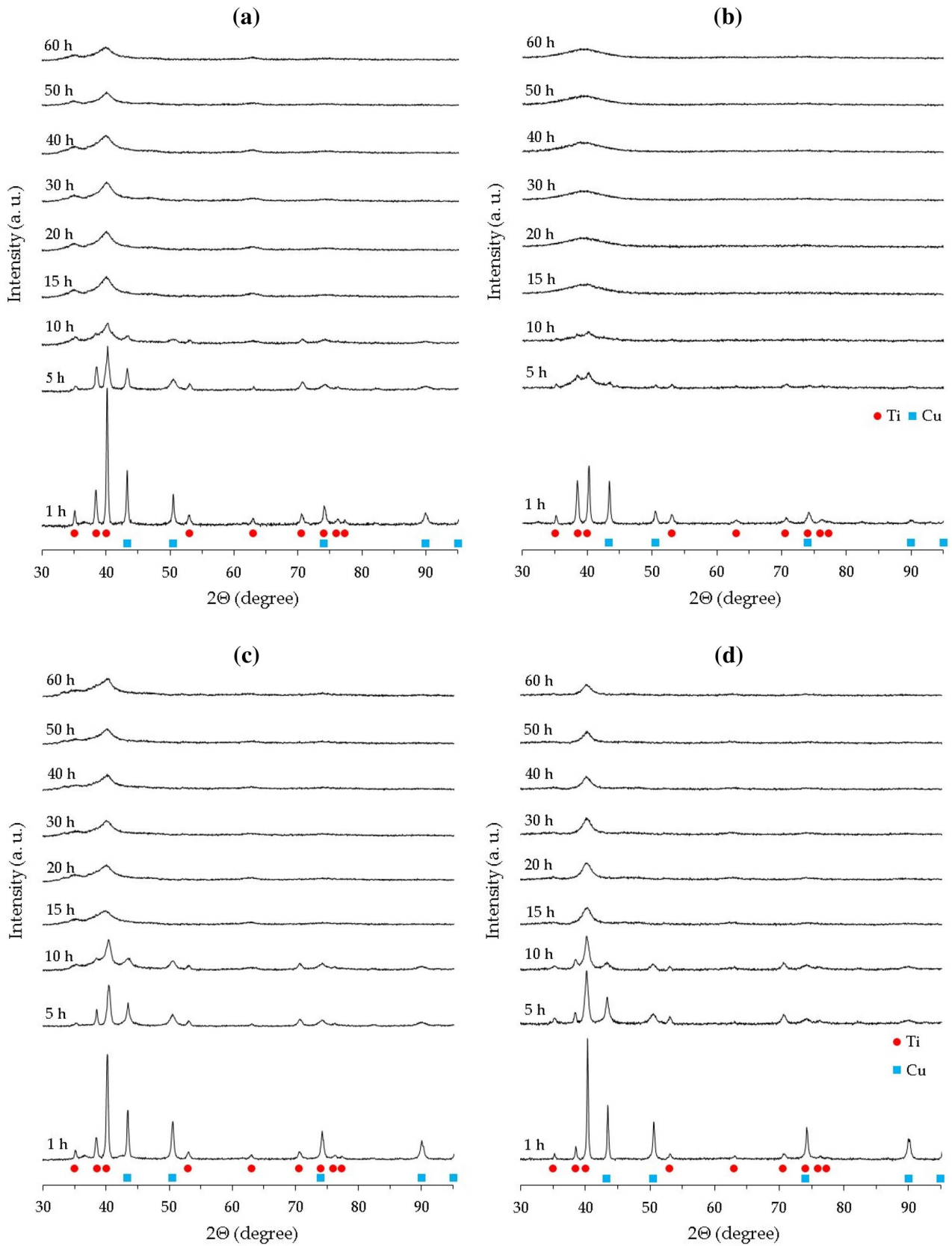


Fig. 5 XRD patterns of (a) $Ti_{90}Cu_{10}$, (b) $Ti_{80}Cu_{20}$, (c) $Ti_{70}Cu_{30}$ and (d) $Ti_{60}Cu_{40}$ alloys milled for periods between 1 and 60 h

the amorphous phases appears with a maximum around $2\Theta = 40^\circ$. The percentage of the amorphous phase increases with milling time, as evidenced by the broadening of the halo.

In Fig. 6 it can be seen that in all the alloys milled for 30 h, the details in the diffractograms around 40° belong to the maximum point of the amorphous phase peak. A clear difference can be distinguished between the amorphized $\text{Ti}_{80}\text{Cu}_{20}$ alloy with a vast low-intensity peak that begins at about 32° and ends at about 48° and the other alloys in which a broad peak appears but with a much greater intensity that denotes the presence of a nanocrystalline or crystalline phase.

In order to corroborate the presence of amorphous phases, transmission electron microscopy (TEM) has been used to study the $\text{Ti}_{80}\text{Cu}_{20}$ alloy milled for 10 and 30 h (Fig. 7).

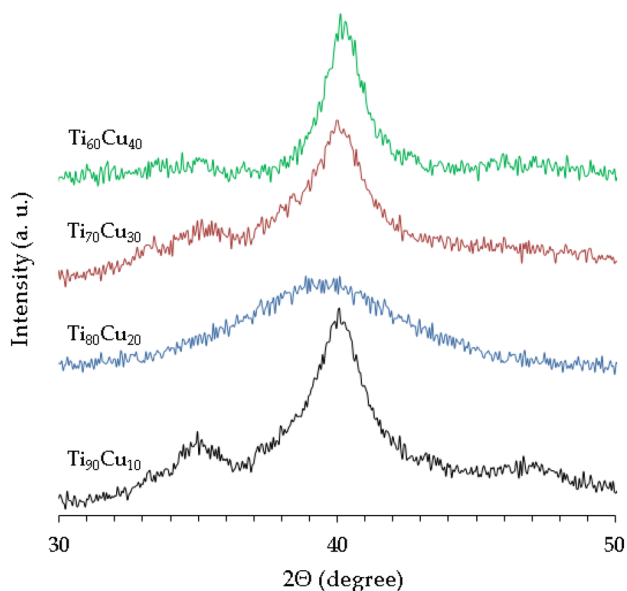
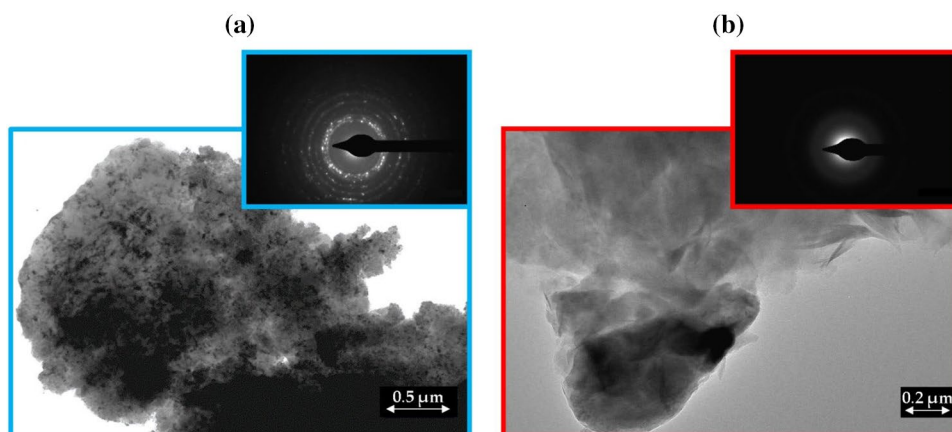


Fig. 6 Detail of XRD patterns of $\text{Ti}_{90}\text{Cu}_{10}$, $\text{Ti}_{80}\text{Cu}_{20}$, $\text{Ti}_{70}\text{Cu}_{30}$, and $\text{Ti}_{60}\text{Cu}_{40}$ alloys milled for 30 h

Fig. 7 TEM micrographs and corresponding diffraction patterns of the $\text{Ti}_{80}\text{Cu}_{20}$ alloy milled for (a) 10 and (b) 30 h, showing (a) nanocrystalline and (b) amorphous phase



In the case of powders milled for ten h, a nanocrystalline microstructure with remains of the amorphous phase is observed. On the contrary, after 30 h, the crystalline and nanocrystalline phases have entirely disappeared, and only the presence of the amorphous phase can be observed.

3.3 Stability of the Amorphous State

To evaluate the behavior at high temperatures of the alloy that has been completely amorphized ($\text{Ti}_{80}\text{Cu}_{20}$), a study has been carried out using DSC (Fig. 8). The alloy milled for one h shows a behavior without the presence of endo or exothermic reactions. On the contrary, after ten h of milling, an exothermic peak, possibly related to cold crystallization from the small amounts of amorphous phase formed during mechanical alloying, appears. This exothermic peak has a higher intensity for the powder milled during 15 h. After 20 and 30 h of milling, in addition to the exothermic peak, an endothermic peak that corresponds to the glass transition region appears. In long-term milling (60 h), the glass transition temperature (T_g) is observed at 350°C and the cold crystallization temperature (T_x) at 395°C . According to these results, these powders can have a suitable temperature for their consolidation, using conventional techniques, of around 350°C .

This DSC study has been complemented with analysis by XRD (Fig. 9) at different temperatures (340 , 390 , 420 , and 500°C) of the $\text{Ti}_{80}\text{Cu}_{20}$ alloy milled for 30 h.

Up to the temperature of 340°C , the sample does not show any structural change compared to powder at room temperature, without heating: The powder maintains its amorphous structure without signs of crystallization. From 390°C , the amorphous phase begins to crystallize, showing some crystalline peaks. The intensity of the peaks increases with increasing temperature. Finally, for the temperature of 500°C , main peaks ($2\Theta = 39.7^\circ$ and 43.5°) and secondary peaks of the intermetallic compound Ti_2Cu (JCPDS Number: 01-072-0441) and some peaks, with lower intensity, in

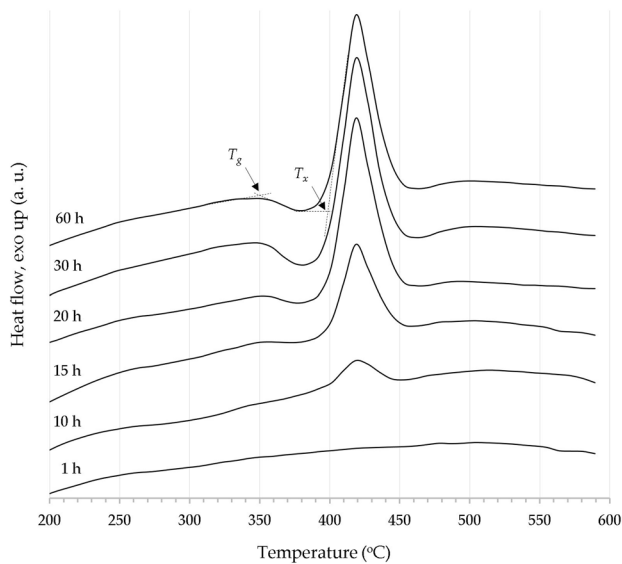


Fig. 8 DSC of $\text{Ti}_{80}\text{Cu}_{20}$ powders milled for 1 h, 10 h, 15 h, 20 h, 30 h, and 60 h

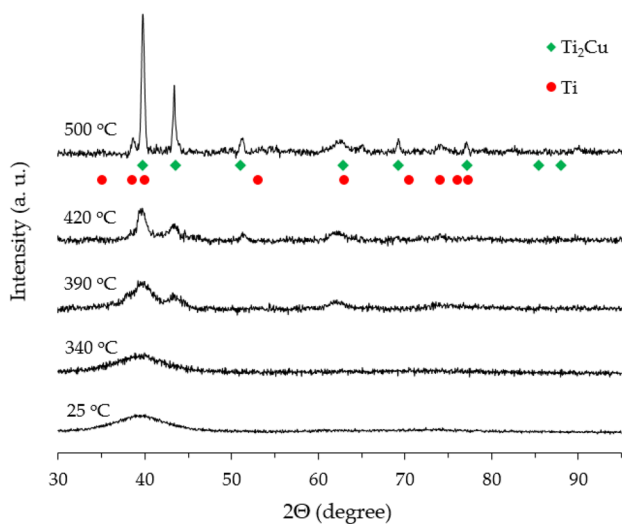


Fig. 9 XRD patterns of $\text{Ti}_{80}\text{Cu}_{20}$ alloy milled for 30 h and heated to 25, 340, 390, 420, and 500 °C

the positions corresponding to Ti (JCPDS Number: 00-044-1291) can be distinguished. It is expected since both phases appear under equilibrium conditions for the $\text{Ti}_{80}\text{Cu}_{20}$ alloy at temperatures below 790 °C.

4 Conclusions

In this work, the effect of the mechanical alloying process on the microstructure and the possibility of amorphization of the $\text{Ti}_x\text{Cu}_{100-x}$ ($x = 90, 80, 70,$ and 60) alloys have

been studied. A $\text{Ti}_{80}\text{Cu}_{20}$ alloy was produced in amorphous form after 30 h of high-energy milling. The pure Ti and Cu particles have been mixed, homogenized and hardened throughout the manufacturing process and the particles' $D(0.5)$ size has decreased from 28.19 μm to 5.81 μm . The amorphous phase is stable up to 340 °C, appearing in the glass transition region at 395 °C. At higher temperatures, the crystallization of the amorphous phase produces an intermetallic compound, Ti_2Cu , and pure titanium.

Acknowledgements University of Seville Research Funding Programme funded this research through the research project 2020/00000647.

Funding Open Access funding provided thanks to the CRUE-CSIC agreement with Springer Nature.

Open Access This article is licensed under a Creative Commons Attribution 4.0 International License, which permits use, sharing, adaptation, distribution and reproduction in any medium or format, as long as you give appropriate credit to the original author(s) and the source, provide a link to the Creative Commons licence, and indicate if changes were made. The images or other third party material in this article are included in the article's Creative Commons licence, unless indicated otherwise in a credit line to the material. If material is not included in the article's Creative Commons licence and your intended use is not permitted by statutory regulation or exceeds the permitted use, you will need to obtain permission directly from the copyright holder. To view a copy of this licence, visit <http://creativecommons.org/licenses/by/4.0/>.

References

1. Klement W, Willens R H, and Duwez P, *Nature* 187 (1960) 869, <https://doi.org/10.1038/187869b0>
2. Urban P, Cuevas F G, Montes J M, and Cintas J, *Materials Science Forum* 730 (2013) 739–744, <https://doi.org/10.4028/www.scientific.net/MSF.730-732.739>
3. Urban P, Ternero Fernández F, Aranda Louvier R M, Astacio López R, and Cintas Físico J, *Key Engineering Materials* 876 (2021) 7 <https://doi.org/10.4028/www.scientific.net/KEM.876.7>
4. Astacio López R, Aranda Louvier R M, Urban P, Ternero Fernández F, and Montes Martos J M, *Key Engineering Materials* 876 (2021) 19, <https://doi.org/10.4028/www.scientific.net/KEM.876.19>
5. Urban P, Sanchez Caballero E, Ternero Fernández F, Viña Reina F J, Gomez Cuevas F, *Key Engineering Materials* 772 (2018) 118, <https://doi.org/10.4028/www.scientific.net/KEM.772.118>
6. An Y, Hou G, Chen J, Zhao X, Liu G, Zhou H, and Chen J, *Vacuum* 107 (2014) 132, <https://doi.org/10.1016/j.vacuum.2014.04.021>
7. Ketov S V, Joksimovic R, Xie G, Trifonov A, Kurihara K, and Louzguine-Luzgin D V, *Heliyon* 3 (2017) 228, <https://doi.org/10.1016/j.heliyon.2016.e00228>
8. Aranda Louvier R M, Astacio López R, Ternero Fernández F, Urban P, and Cuevas F G, *Key Engineering Materials* 876 (2021) 25, <https://doi.org/10.4028/www.scientific.net/KEM.876.25>
9. Hua N, Liao Z, Chen W, Huang Y, and Zhang T, *Journal of Alloys and Compounds* 725 (2017) 403, <https://doi.org/10.1016/j.jallcom.2017.07.167>

10. Urban P, Ternero Fernández F, Sánchez Caballero E, Nandyala S, Montes J M, and Cuevas F G, *Metals* 9(11) (2019) 1140, <https://doi.org/10.3390/met9111140>
11. Li M C, Jiang M Q, Jiang F, He L, and Sun J, *Scripta Materialia* 138 (2017) 120, <https://doi.org/10.1016/j.scriptamat.2017.05.046>
12. Lin H K, and Hong S Z, *Journal of Alloys and Compounds* 731 (2018) 248, <https://doi.org/10.1016/j.jallcom.2017.09.273>
13. Ram Lim K, Man Park J, Jun Kim S, Lee E S, Tae Kim W, Gebert A, Eckert J, and Hyang Kim D, *Corrosion Science* 66 (2013) 1, <https://doi.org/10.1016/j.corsci.2012.09.018>
14. A. Zarebidaki, A. Seifoddini, T. Rabizadeh, *Journal of Alloys and Compounds* 736 (2018) 17, <https://doi.org/10.1016/j.jallcom.2017.11.138>
15. N.W. Khun, H. Yu, Z.Z. Chong, P. Tian, Y. Tian, S.B. Tor, E. Liu, *Materials and Design* 92 (2016) 667, <https://doi.org/10.1016/j.matdes.2015.12.050>
16. S. Cardinal, J.M. Pelletier, M.Eisenbart, U.E. Klotz, *Materials Science & Engineering A* 660 (2016) 158, <https://doi.org/10.1016/j.msea.2016.02.078>
17. Y. Saotome, Y. Fukuda, I. Yamaguchi, A. Inoue, *Journal of Alloys and Compounds* 434-435 (2007) 97, <https://doi.org/10.1016/j.jallcom.2006.08.126>
18. D. L.P. Feil, P.R. Silva, D.P. Bernardon, T.B. Marchesan, M. Sperandio, L.H. Medeiros, *Electric Power Systems Research* 144 (2017) 268-279, <https://doi.org/10.1016/j.epsr.2016.12.015>
19. F.R. Ismagilov, V.E. Vavilov, A.H. Miniyarov, R.R. Urazbakhtin, *International Journal of Hydrogen Energy* 43(24) (2018) 11180, <https://doi.org/10.1016/j.ijhydene.2018.04.185>
20. K. Zhou, Ch. Chen, Y. Liu, S. Pang, N. Hua, W. Yang, T. Zhang, *Intermetallics* 90 (2017) 81, <https://doi.org/10.1016/j.intermet.2017.07.007>
21. Ch.-W. Chi, Y.-L. Deng, J.-W. Lee, Ch.-P. Lin, *Journal of the Formosan Medical Association* 116 (2017) 373, <https://doi.org/10.1016/j.jfma.2016.07.003>
22. K. Pajora, T. Kozieł, G. Cios, P. Błyskun, P. Bała, A. Zielińska-Lipieca, *Journal of Non-Crystalline Solids* 496 (2018) 42, <https://doi.org/10.1016/j.jnoncrysol.2018.05.034>
23. A. Monfared, A. Ghaee, S. Ebrahimi-Barough, *Colloids and Surfaces B: Biointerfaces* 170 (2018) 617, <https://doi.org/10.1016/j.colsurfb.2018.06.060>
24. D. Li, Z.W. Zhu, A.M. Wang, H.M. Fu, H. Li, H.W. Zhang, H.F. Zhang, *Journal of Materials Science & Technology* 34 (2018) 708, <https://doi.org/10.1016/j.jmst.2017.07.008>
25. G. Xie, H. Kanetaka, H. Kato, F. Qin, W. Wang, *Intermetallics* 105 (2019) 153, <https://doi.org/10.1016/j.intermet.2018.12.002>
26. E. Zhang, X. Wang, M. Chen, B. Hou, *Materials Science and Engineering C* 69 (2016) 1210, <https://doi.org/10.1016/j.msec.2016.08.033>
27. H. Wang, X. Shu, M. Guo, D. Huang, Z. Li, X. Li, B. Tang, *Surface & Coatings Technology* 235 (2013) 235, <https://doi.org/10.1016/j.surfcoat.2013.07.038>
28. J. Liu, F. Li, C. Liu, H. Wang, B. Ren, K. Yang, E. Zhang, *Materials Science and Engineering C* 35 (2014) 392, <https://doi.org/10.1016/j.msec.2013.11.028>
29. J. Fornell, E. Pellicer, N. Van Steenberge, S. Gonzalez, A. Gebert, S. Surinach, M.D. Baro, J. Sort, *Materials Science & Engineering A* 559 (2013) 159, <https://doi.org/10.1016/j.msea.2012.08.058>
30. K.H.J. Buschow, *Acta metal.* 31 (1983) 155
31. V.V. Savin, A. Chaika, *Powder Metallurgy and Metal Ceramics* 37(7-8) (1998) 448
32. K.D. Machado, G.A. Maciel, D.F. Sanchez, J.C. de Lima, P. Jóvári, *Solid State Communications* 150 (2010) 1674, <https://doi.org/10.1016/j.ssc.2010.06.027>
33. M.S. Al-Assiri, A. Alolah, A. Al-Hajry, M. Bououdina, *Rev. Adv. Mater. Sci.* 18 (2008) 241
34. N.F. Shkodich, S.G. Vadchenko, A.A. Nepapushev, D. Yu Kovalev, I.D. Kovalev, S. Ruvimov, A.S. Rogachev, A.S. Mukasyan, *Journal of Alloys and Compounds* 741 (2018) 575, <https://doi.org/10.1016/j.jallcom.2018.01.062>
35. C. Politis and W. L. Johnson, *Journal of Applied Physics* 60 (1986) 1147, <https://doi.org/10.1063/1.337359>

Publisher's Note Springer Nature remains neutral with regard to jurisdictional claims in published maps and institutional affiliations.